ACS Catalysis

Research Article

pubs.acs.org/acscatalysis

Formic Acid As a Hydrogen Storage Medium: Ruthenium-Catalyzed Generation of Hydrogen from Formic Acid in Emulsions

Miklos Czaun,* Alain Goeppert, Jotheeswari Kothandaraman, Robert B. May, Ralf Haiges, G. K. Surya Prakash,* and George A. Olah*

Loker Hydrocarbon Research Institute and Department of Chemistry, University of Southern California, University Park Campus, Los Angeles, California 90089, United States

Supporting Information

ABSTRACT: Formic acid is decomposed to H_2 and CO_2 in the presence of $RuCl_3$ and triphenylphosphines in an emulsion. In situ formed ruthenium carbonyls, such as $[Ru(HCO_2)_2(CO)_2(PPh_3)_2]$ (**1**), $[Ru(CO)_3(PPh_3)_2]$ (**2**), and $[Ru_2(HCO_2)_2(CO)_4(PPh_3)_2]$ (**3**), and a large cluster, involving a Ru_{12} core, were identified and structurally characterized from the reaction mixtures. The catalytic activity of the mono and binuclear complexes was also investigated and it was found that $[Ru_2(HCO_2)_2(CO)_4(PPh_3)_2]$ (**3**) shows high stability even at elevated temperatures and pressures and its activity is 1 order of magnitude lower than those measured for the mononuclear complexes. It was also attempted to use $[Ru(HCO_2)_2(CO)_2(PPh_3)_2]$ (**1**) as a catalyst for the hydrogenation of CO_2 to formic acid under neutral conditions. Although the reduction of CO_2 did not take place, the conversion of $[Ru(HCO_2)_2(CO)_2(PPh_3)_2]$ (**1**) to an unexpected carbonate, $[Ru(CO_3)(CO)_2(PPh_3)_2]\cdot H_2O$ was observed.

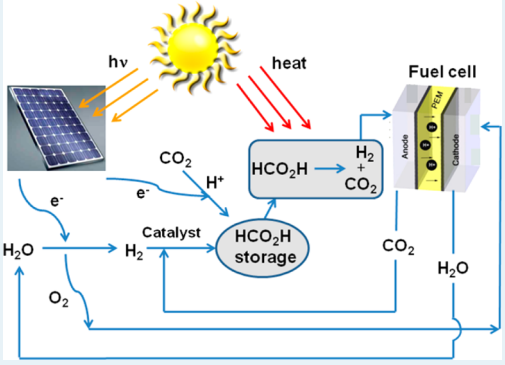

KEYWORDS: *hydrogen storage, formic acid decomposition, ruthenium chloride, homogeneous catalyst, emulsion*

Burning of fossil fuels, mainly coal, natural gas, and oil, to fulfill the ever increasing energy demand of humankind has resulted in the accumulation of carbon dioxide in the atmosphere where its concentration will exceed 400 ppm this year. The global anthropogenic carbon dioxide emissions rose by more than 5% in 2010, representing the largest increase per annum in the last two decades.[1] The finite nature of fossil fuels and the increasingly severe consequences of high carbon dioxide levels in the atmosphere, such as global warming and seawater acidification calls for a sustainable energy cycle to replace our existing one. It can be expected that as a result of the conscious effort to decrease anthropogenic greenhouse gas emission, the contribution of renewable energy sources to the total energy production will be increasing.

Extensive exploitation of renewable energy sources like solar, wind and hydro in addition to the utilization of nuclear power will provide enough energy for the future and predictions indicate that humankind may indeed face energy storage and transportation problems as well as shortage of carbon sources rather than an actual energy shortage.[2] A more efficient utilization of our limited fossil fuel sources may delay the difficulties associated with carbon shortage.[3−5]

Using electricity from renewable sources to produce hydrogen by splitting water followed by storage and then utilization of hydrogen to generate electricity on demand would be a "clean" approach to store energy since the only product generated by burning hydrogen is water, an environmentally benign compound. Although this technology would not emit harmful side products, storing and transporting hydrogen in large quantities is quite challenging because of its volatile, flammable, and explosive nature.[6]

Numerous substances, for example, ammonia borane,[7] alkali borohydrides,[8] hydrous hydrazine,[8] methane, methanol,[6] etc., have been suggested for chemical energy storage in addition to hydrogen. However, the practical applicability of some of these substances may be hampered because of their relatively high price, toxicity, or safety issues.

Formic acid (FA) is a low volatility, low toxicity organic acid,[9] which can be synthesized by decomposition of biomass, or by catalytic hydrogenation,[10−12] and direct electrochemical reduction[13−15] of carbon dioxide. Subsequently, FA can be decomposed to a mixture of H_2 and CO_2 resulting in a "carbon neutral" energy/hydrogen storage system (Figure 1).[16−23] The required CO_2 can also be captured from industrial streams or even directly from air.[24−28]

The decomposition of FA can follow two main pathways: (a) decarbonylation resulting in carbon monoxide and water (1:1) and (b) decarboxylation providing a 1:1 mixture of carbon dioxide and hydrogen (Scheme 1). The latter mixture can be used directly as a feedgas for hydrogen/air fuel cells,[29,30] and the hydrogen depleted exhaust may be recycled for FA synthesis.

Received: September 9, 2013
Revised: November 27, 2013
Published: December 4, 2013

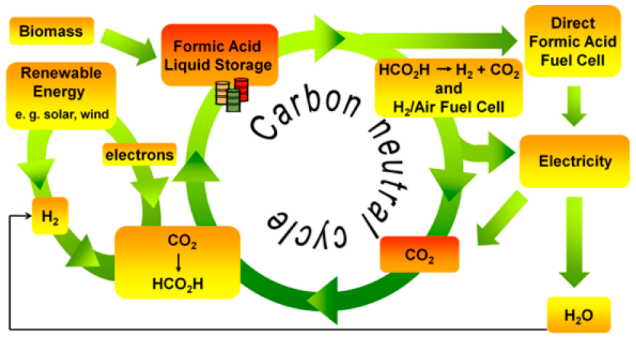

Figure 1. Carbon neutral energy storage using FA as storage medium.

Scheme 1. Decomposition Pathways of FA: (a) Decarbonylation and (b) Decarboxylation

$$CO + H_2O \xleftarrow{(a)} HCO_2H \xrightarrow{(b)} H_2 + CO_2$$

Since CO may deactivate the catalysts of fuel cells, the development of high activity homogeneous catalysts for the selective decarboxylation of FA suppressing the decarbonylation has received increasing attention.[17−19,23]

Ruthenium catalysts developed by Beller et al., which are formed in situ from $[RuCl_2(benzene)]_2$ in the presence of 1,2-bisdiphenylphosphinoethane (dppe) and a variety of amine additives e.g. Et_3N exhibited excellent performance for FA decomposition. For example, the $[RuCl_2(benzene)]_2$/dppe/dimethyloctylamine (DMOA) system showed one of the highest activity (TOF = 16000 h^{-1} 60 °C) reported for hydrogen generation from FA.[31]

Another outstanding example was reported by Laurenczy et al. in 2009 using $[Ru(H_2O)_6](tos)_2]$, $[Ru(H_2O)_6](tos)_3]$, or $RuCl_3$ in an aqueous solution of FA/Na-formate (9:1) (TOF = 460 h^{-1}) and *meta*-trisulfonated triphenylphosphine (TPPTS) as catalyst precursors.[32]

Although these systems showed excellent performance, their large scale application may bring up feasibility concerns due to the relatively high cost of the catalyst precursors.

In addition to this, volatile amine additives (e.g., Et_3N) may contaminate the gaseous products, necessitating gas purification before their utilization in a fuel cell. To avoid this problem, application of less volatile amines (e.g., $HexNMe_2$) has been already suggested.[16,31]

For the wide practical application of continuous hydrogen generation from FA, the development of more cost-effective systems would however be essential for example (a) by using less expensive and stable ligands that can be produced on a large scale or (b) development of active catalysts using nonprecious metals. The highest activity and productivity results (TOF of 9425 h^{-1} at 80 °C) for nonprecious metal-based catalyst systems were observed using $P(CH_2CH_2PPh_2)_3$ as a ligand and $Fe(BF_4)_2{\cdot}6H_2O$ as the metal precursor.[21] However its long-term stability remains to be studied.

The aim of this work is to gain an insight into the underlying chemistry of formic acid decomposition in the presence of cost-effective and commercially available ligands (e.g., PPh_3) and $RuCl_3$, through identification of organometallic species formed in situ under relatively harsh conditions, such as aqueous acidic solutions at elevated temperatures.

Triphenyl phosphine (PPh_3) is a commonly used P-donor ligand in organometallic chemistry. However, its poor solubility in water disfavors its application in aqueous reaction mixtures. On the other hand, transition metal salts like $RuCl_3$, as well as FA and sodium formate are mainly soluble in water. Substitution of the aromatic rings in triphenyl phosphine may not only change the electron density on the phosphorus atom but may also modify the solubility of the ligand in organic and aqueous solutions as it was demonstrated with TPPTS ligand.[32]

The miscibility of aqueous and organic phases can be enhanced by the addition of surfactants to form emulsions. Even though these emulsions may not be stable over the entire reaction time due to dramatic changes in the composition of the reaction mixture, the initial presence of an emulsion can provide the proper medium for the in situ formation of active catalytic species. The role of such emulsions in the decomposition of FA has now been explored.

The aqueous solution of FA, sodium formate and $RuCl_3$ was added dropwise to the vigorously stirred mixture of toluene, PPh_3 and sodium dodecyl sulfate (SDS) followed by sonication of the formed emulsion for 15 min at room temperature. The light brown emulsion was then transferred to a high pressure Monel autoclave and heated to temperatures of 90 to 117 °C. The internal temperature of the reactor and the pressure of the gaseous product was recorded using Lab View and the rate of decomposition was calculated on the basis of the pressure versus time profiles (Figure 2) at various temperatures (e.g.,

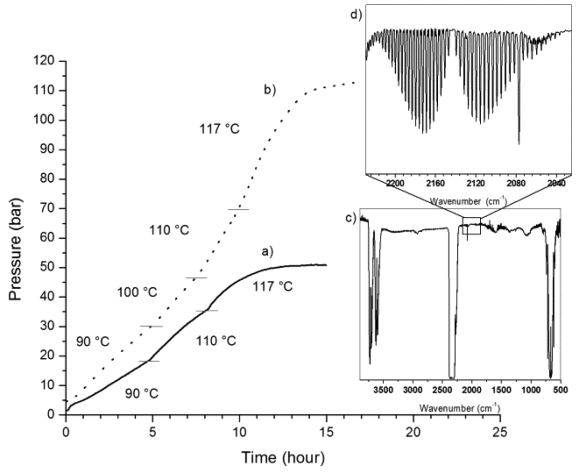

Figure 2. Pressure vs time diagram for the FA decomposition in the presence of $RuCl_3$−PPh_3−SDS: (a) first run and (b) second run. FTIR spectra of gaseous products (c and d).

1.692 × 10^{-5} M·s^{-1} at 90 °C, Table 1). To determine the selectivity of the decomposition, the chemical composition of the gas mixture was analyzed by gas chromatography using a thermal conductivity detector (TCD) and in some cases by Fourier transform infrared spectroscopy (FTIR) as well.

The high selectivity of the reaction was reflected by the lack of CO peak in the chromatogram as illustrated in Supporting Information Figure S1a. Using FTIR spectroscopy, a more sensitive analytical method, only traces of CO were detected in the gas mixture (Figure 2c and d). After the first run, 97% FA was added and the rate of decomposition was measured (2.001 × 10^{-5} M·s^{-1} at 90 °C). As Figure 2 illustrates, the system showed a higher reaction rate in the second run due to the formation of more active species. However, gas chromatographic measurements revealed the accumulation of 0.25% CO (Supporting Information Figure S1b).

dx.doi.org/10.1021/cs4007974 | ACS Catal. 2014, 4, 311−320

Table 1. Reaction Rates of FA Decomposition in the Presence of Various Phosphine Ligands and Composition of Gaseous Products

	phosphine[a]	t (°C)	$10^6 \times$ reaction rate ($M \cdot s^{-1}$)	gas composition (%)[b]		
				H_2	CO_2	CO
1[c]	PPh_3	90	16.920	54.20	45.80	nd
2[d]	PPh_3	90	20.010	56.19	43.56	0.25
3[c]	$P(C_6H_4{-}CH_3)_3$	90	13.990	54.71	45.29	nd
4[d]	$P(C_6H_4{-}CH_3)_3$	90	7.314	55.70	44.10	0.20
5[c]	$PPh_3 \cdot HBr$	90	30.172	53.46	46.54	nd
6[d]	$PPh_3 \cdot HBr$	90	61.243	51.31	48.69	nd
7[c]	$P(C_6H_4{-}Cl)_3$	90	16.288	53.60	46.40	nd
8[c]	$O{=}PPh_3$[e]	90	4.428	54.17	45.83	nd
9[d]	$O{=}PPh_3$[e]	90	1.096	54.01	45.99	nd
10[c]	$P(C_6H_4{-}F)_3$	90	0.579	48.67	47.57	3.76
11[c]	$P(C_6H_4{-}F)_3$	110	0.997			
12	no catalyst[f]	117	0.377	39.39	50.58	10.1

[a]$[RuCl_3]$ = 2.43 mM, [Phosphine] = 5.0 mM, [FA] = 3.6 M, $[HCO_2Na]$ = 0.4 M, [SDS] = 19.65 mM, 25 mL aqueous solution, 5 mL toluene. [b]Determined by gas chromatography using TCD, nd: no CO could be detected. [c]First run. [d]Second run. [e]No SDS was added. [f][FA] = 9 × $[HCO_2Na]$ = 3.6 M, 25 mL aqueous solution, no catalyst, Table S1 shows the reaction rates at variable temperatures (see Supporting Information).

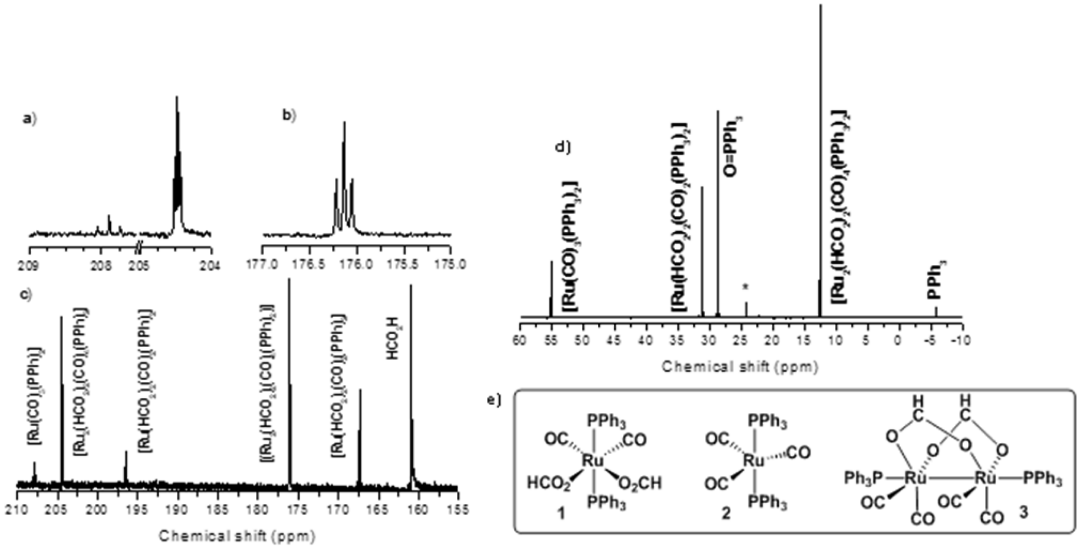

Figure 3. ^{13}C NMR (a–c) and ^{31}P NMR spectra (d) of crude catalyst mixture and the stucture of the Ru complexes formed in situ (e) (* = unidentified species).

In another experiment, the emulsion was separated by centrifugation directly after the first run and the aqueous phase was extracted with toluene. In order to understand the nature of the organometallic species formed in situ that may contribute to the catalytic activity, the identification of Ru-complexes was carried out directly from the crude reaction mixture. The ^1H NMR spectra of the crude extract showed the presence of unreacted FA and Na-formate, ruthenium coordinated formate, the mixture of PPh_3 and $O{=}PPh_3$. ^{13}C NMR studies (Figure 3) revealed the presence of $[Ru(HCO_2)_2(CO)_2(PPh_3)_2]$ (**1**) (196.7 ppm (t, 11.2 Hz, CO), 167.5 ppm (s, HCO_2^-)), $[Ru(CO)_3(PPh_3)_2]$ (**2**) (208.0 ppm (t, 16.1 Hz, CO)), and $[Ru_2(HCO_2)_2(CO)_4(PPh_3)_2]$ (**3**) complex (204.7 ppm, (t, 4.1 Hz, CO), 176.3 ppm (t, 8.2 Hz, HCO_2^-)).

^{31}P NMR measurements (Figure 3d) also confirmed the presence of complex $[Ru_2(HCO_2)_2(CO)_4(PPh_3)_2]$ (**3**), $[Ru(HCO_2)_2(CO)_2(PPh_3)_2]$ (**1**), and $[Ru(CO)_3(PPh_3)_2]$ (**2**) at 12.6, 31.2, and 55.6 ppm, respectively. Interestingly, Wills et al. have not reported the presence of **1** and **2** in the reaction between FA and $RuCl_3$, $[RuCl_2(DMSO)_4]$ or $[RuCl_2(NH_3)_6]$ in the presence of PPh_3 and Et_3N. Instead, the authors described the formation of the binuclear $[Ru_2(HCO_2)_2(CO)_4(PPh_3)_2]$ (**3**) and the tetranuclear $[Ru_4(HCO_2)_4(CO)_8(PPh_3)_2]$ complex; the latter being a fairly unstable species.

In our system, the lack of a peak at 5.8 ppm (^{31}P NMR) revealed the absence of tetranuclear Ru species $[Ru_4(HCO_2)_4(CO)_8(PPh_3)_2]$. However, it should be noted here that ^{31}P NMR measurements of the crude reaction mixture also revealed the presence of an unidentified phosphorus containing species with a peak at 24.3 ppm.

The isolated crude catalyst mixture was washed with hexane and recrystallized from chloroform by pentane diffusion. The obtained yellow prisms were characterized by various spectroscopic methods (Supporting Information Figure S2 and Figure 3) and subjected to X-ray crystal structure analysis.

The ^1H, ^{13}C, and ^{31}P NMR measurements revealed that these prisms were complex **1**. The FTIR spectrum of the yellow prisms collected in carbon tetrachloride exhibits intense bands at 2052.8, 1991.1, 1957.0 cm^{-1} due to the stretching vibration

dx.doi.org/10.1021/cs4007974 | ACS Catal. 2014, 4, 311–320

Table 2. Crystallographic Parameters for $[Ru(HCO_2)_2(CO)_2(PPh_3)_2]\cdot 2CHCl_3$, $[Ru(CO)_3(PPh_3)_2]\cdot$toluene, and $[Ru_{12}C_{30}H_{14}Na_2O_{50}\cdot 6(C_{18}H_{15}OP)\cdot 2(C_7H_8)\cdot 4(H_2O)]$

	1·2CHCl$_3$	**2**·toluene	**4**
formula	$C_{42}H_{34}Cl_6O_6P_2Ru$	$C_{42.20}H_{34}Cl_{0.30}O_{2.71}P_2Ru$	$C_{76}H_{66}NaO_{30}P_3Ru_6$
MW (g/mol)	1010.40	757.84	2181.61
space group	$P\bar{1}$	$P2_1/c$	$P\bar{1}$
a (Å)	9.915(2)	17.7301(6)	16.3958(9)
b (Å)	11.919(2)	12.3659(4)	17.5531(9)
c (Å)	20.194(4)	18.3431(6)	17.6055(9)
α (deg)	97.563(3)	90	101.4600(10)
β (deg)	91.490(3)	102.9990(10)	113.7560(10)
γ (deg)	112.378(3)	90	107.5850(10)
V (Å^3)	2180.0(8)	3918.6(2)	4111.9(4)
Z	2	4	2
T (K)	133(2)	100(2)	100.(2)
λ (Å)	0.71073	0.71073	0.71073
D_{calcd} (g/cm^3)	1.539	1.285	1.762
μ (mm^{-1})	0.847	0.554	1.220
crystal size (mm)	0.15 × 0.15 × 0.15	0.32 × 0.24 × 0.15	0.570 × 0.080 × 0.080
reflections collected	13889	94892	99952
independent reflections	9554 [R(int) = 0.0344]	13990 [R(int) = 0.0365]	24604 [R(int) = 0.0275]
goodness-of-fit on F^2	1.047	1.132	1.088
Final R indices [$I > 2\sigma(I)$]	R1 = 0.0447, wR2 = 0.0802	R1 = 0.0566, wR2 = 0.1579	R1 = 0.0279, wR2 = 0.0602
R indices (all data)	R1 = 0.0720, wR2 = 0.1004	R1 = 0.0739, wR2 = 0.1704	R1 = 0.0391, wR2 = 0.0648

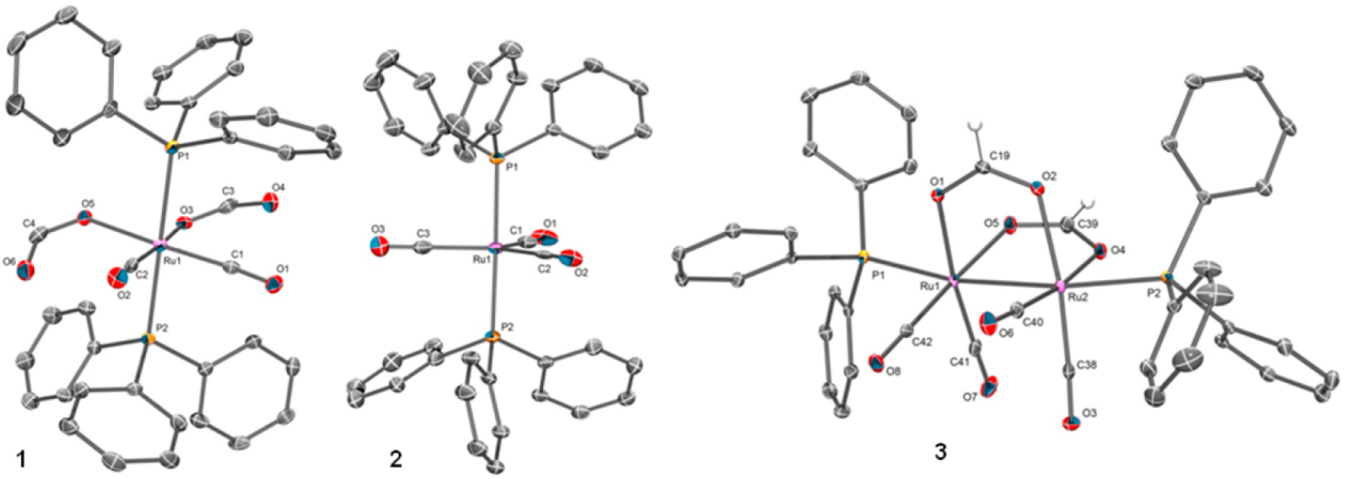

Figure 4. Crystal structure of complexes **1**, **2**, and **3**. Hydrogen atoms and the solvent molecules have been omitted for clarity. Thermal ellipsoids are drawn at the 50% probability level.

of coordinated CO ligands. Furthermore, the bands at 1606.6 and 1300.6 cm^{-1} can be attributed to the asymmetric and symmetric carbonyl stretching vibration of unidentate formate ligand, respectively (Supporting Information Figure S2). These values are in good agreement with those reported by Johnson et al. for the same compound (**1**).[33]

The X-ray crystal structure of the obtained yellow-colored prisms revealed that the mononuclear hexacoordinated Ru(II) compound $[Ru(HCO_2)_2(CO)_2(PPh_3)_2]$ crystallizes together with two molecules of chloroform solvent in the triclinic space group $P\bar{1}$ with two symmetry related units in the unit cell (Z = 2).

Further crystallographic parameters are listed in Table 2. The crystal structure of **1** is depicted in Figure 4. In this compound, the ruthenium atom is hexa-coordinated by two triphenylphosphine, two carbonyl and two formate ligands. The arrangement is derived from an octahedron with both PPh_3 ligands occupying the axial positions and the formate and carbonyl ligands arranged cis in the equatorial positions. The Ru atom lies in the equatorial plane formed by the oxygen atoms O(3) and O(5) of the formate ligands and the carbon atoms C(1) and C(2) of the carbonyl ligands.

Although it has been reported by Johnson et al.[33] that the reaction between $[Ru(CO)_3(PPh_3)_2]$ and formic acid under toluene reflux results in the formation of **1**, the same complex has never been synthesized directly in a reaction between $RuCl_3$, PPh_3 and formic acid in which the acid acts as both, carbonylating as well as reducing agent. Moreover, the X-ray crystal structure of $[Ru(HCO_2)_2(CO)_2(PPh_3)_2]$ had not been established until our current studies.

After isolating $[Ru(HCO_2)_2(CO)_2(PPh_3)_2]$ from the chloroform solution by pentane diffusion, the supernatant was evaporated and redissolved in toluene. Hexane was diffused into the toluene solution and stored at 0 °C for a week giving

dx.doi.org/10.1021/cs4007974 | ACS Catal. 2014, 4, 311−320

Scheme 2. Formation of Complexes 1−4[a]

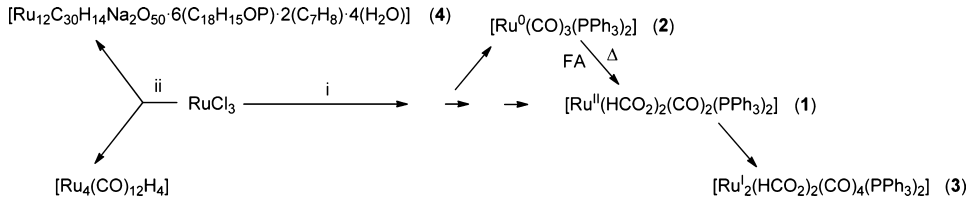

[a]Reaction conditions: (i) FA, Na-formate, PPh_3, toluene, SDS, 90 °C; (ii) FA, Na-formate, $O = PPh_3$, toluene, 90 °C.

two different types of crystals: yellow plates and yellow blocks. The yellow plates were found suitable for single crystal X-ray diffraction and the structure determination revealed the binuclear complex $[Ru_2(HCO_2)_2(CO)_4(PPh_3)_2]$ with two bridging formato ligands (Figure 4). The determined crystallographic parameters of the binuclear ruthenium complex (Supporting Information Table S2) are in good agreement with those reported by Wills et al.[34]

The yellow block-like crystals were identified by single crystal X-ray diffraction as $[Ru(CO)_3(PPh_3)_2]$ (**2**), which crystallizes with one molecule of toluene solvent in the asymmetric unit. The crystal structure of the compound is depicted in Figure 4. The basic geometry of $[Ru(CO)_3(PPh_3)_2]$ is derived from a bipyramidal ligand arrangement around the Ru center with the two PPh_3 groups occupying the axial and the carbonyls in the equatorial positions. The determined X-ray crystal structure of $[Ru(CO)_3(PPh_3)_2]$·toluene suffers from several disorders (see in the Supporting Information).

Collman and Roper[35] reported the first synthesis of $[Ru(CO)_3(PPh_3)_2]$ from $[RuCl_2(CO)_2(PPh_3)_2]$ by reaction with zinc dust. In our reaction, $[Ru(CO)_3(PPh_3)_2]$ may be formed via $[RuCl_2(CO)_2(PPh_3)_2]$ since the latter complex can be a potential intermediate of the reaction between $RuCl_3$, CO and PPh_3 under reductive conditions[35] as described in Scheme 2.

Study of the Performance of $RuCl_3$ for FA Decomposition in the Presence of Triphenylphosphine Derivatives. Performance of catalysts formed from $RuCl_3$ and ortho- and para-substituted triphenylphosphines, triphenylphosphonium bromide and triphenylphosphine oxide (Supporting Information Figure S4) have also been investigated for the decarboxylation of FA in an emulsion. Comparison of reaction rates obtained using P-donor ligands is illustrated in Figure 5 and also given in Table 1.

Apparently, the reaction rate is independent of the electronic effects of the substituents since similar values were obtained for PPh_3, tris(4-chlorophenyl)phosphine and tris(2-tolyl)-phosphine (16.92×10^{-6}, 16.29×10^{-6}, 13.99×10^{-6} M s^{-1}, respectively). Instead, it can be suggested that the solubility of different ligands and the complexes formed in situ in the aqueous phase affects the catalytic activity. This is also supported by the higher activity of the $RuCl_3$−PPh_3·HBr system (30.17×10^{-6} M s^{-1}), where phosphine salt has a relatively good solubility in water compared with nonionic phosphine ligands. On the other hand, $RuCl_3$/tris(4-fluorophenyl)phosphine remained practically inactive even at 110 °C as reflected in its low reaction rate (0.997×10^{-6} M s^{-1}). This system also showed poor selectivity, resulting in a gas mixture containing 3.8% CO.

Thermal decomposition of FA to H_2O and CO (Scheme 1a) can also take place as a side reaction, resulting in higher CO content in the presence of a catalyst which is less active for the

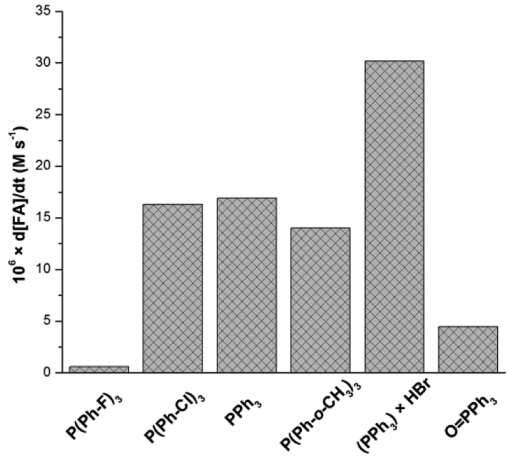

Figure 5. Reaction rates of FA decomposition using triphenylphosphine and derivatives. Conditions: see in Table 1

decarboxylation of FA. A blank experiment was carried out without adding any catalyst to make an adequate comparison on the selectivity of the tested catalysts shown in Table 1. As expected, both the rate of the decomposition and the selectivity (rr = 0.377×10^{-6} M s^{-1} at 117 °C, CO% = 10.1) suffered from the absence of catalyst giving higher CO content than the one measured in the presence of the least selective catalyst precursor, tris(4-fluorophenyl)phosphine, (CO% = 3.76). It can be concluded that the application of a less active catalyst with long reaction times favors the accumulation of CO in the gas mixture.

To explore the robustness of the $RuCl_3$−phosphine system in an emulsion, triphenylphosphine oxide ($O{=}PPh_3$) was used as a ligand to model practical conditions (e.g., PPh_3 is contaminated with $O{=}PPh_3$ impurity, the FA feed contains dissolved oxygen, or both). Although the reaction rate in the presence of $O{=}PPh_3$ was relatively low (4.43×10^{-6} M s^{-1}) at 90 °C the selectivity of the reaction was high, giving a mixture of H_2 and CO_2 (Table 1) with no traces of CO.

It is very unlikely that $O{=}PPh_3$ can be converted into PPh_3 even under reductive conditions and that Ru−PPh_3 complexes similar to the ones that were detected when PPh_3 was used directly as a ligand can be formed. In the reaction between $RuCl_3$ and $O{=}PPh_3$ in the presence of FA and sodium formate in the toluene/water biphasic system the formation of $[Ru_4(CO)_{12}H_4]$[18] (toluene phase) and orange-red block-like crystals in the aqueous layer were observed.

On the basis of the ^{31}P NMR results, the presence of any phosphine ligands in the orange-red compound was ruled out (except for $O{=}PPh_3$) while signals at 181.4 and 162.3 ppm in the ^{13}C NMR spectrum can be assigned to carbonyl and carbonate ligands, respectively (Supporting Information Figure S5). IR measurements showed five adsorption bands in the

dx.doi.org/10.1021/cs4007974 | ACS Catal. 2014, 4, 311−320

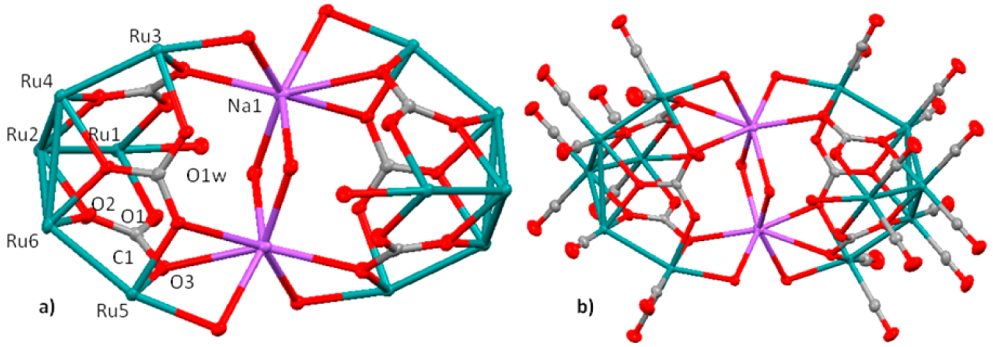

Figure 6. The core structure of the Ru cluster in the crystal structure of ($[Ru_{12}C_{30}H_{14}Na_2O_{50}\ 6(C_{18}H_{15}OP)\ 2(C_7H_8)\ 4(H_2O)]$ (**4**). (a) Hydrogen atoms, water, toluene, triphenylphosphine oxide, and carbon monoxide molecules have been omitted for clarity. (b) Hydrogen atoms, water, toluene, and triphenylphosphine oxide have been omitted for clarity.

Table 3. Comparison of Reaction Rates and Selectivity Using $RuCl_3/PPh_3$ in the Presence of Different Surfactants

				gas composition (%)[b]		
	surfactant	t (°C)	$10^6 \times$ reaction rate ($M \cdot s^{-1}$)	H_2	CO_2	CO
1[a]	SDS	100	69.14	54.20	45.80	nd
2[a]	TBAB	100	26.22	54.49	45.44	0.07
3[a]	MiTMAB	100	9.58	55.80	43.98	0.22
4[c]		100	9.90	52.23	47.47	0.30
5[d]		100	14.09	54.91	44.95	0.15

[a]$[RuCl_3]$ = 2.43 mM, [Phosphine] = 5.0 mM, [FA] = 3.6 M, $[HCO_2Na]$ = 0.4 M, [surfactant] = 19.65 mM, 25 mL aqueous solution, 5 mL toluene. [b]Determined by gas chromatography using TCD. nd: no CO could be detected. [c]No toluene and surfactant was added. [d]No surfactant was added.

region from 2051 to 1922 cm^{-1} (carbonyl ligands) and also a broad adsorption at 1540 cm^{-1} (carbonato) (Supporting Information Figure S6).

The orange-red blocks were subjected to single crystal X-ray diffraction, which showed the presence of a large unexpected Ru carbonato cluster incorporating twelve ruthenium atoms ($[Ru_{12}C_{30}H_{14}Na_2O_{50}{\cdot}6(C_{18}H_{15}OP){\cdot}2(C_7H_8){\cdot}4(H_2O)]$ (**4**), unit cell volume = 4111.9(4) $Å^3$). Crystallographic parameters of the complex are summarized in Table 2. The structure is quite unique because it consist of two identical cluster units $[Ru_6(CO_3)_3(CO)_{12}(OH)(H_2O)_2]$ that are bridged by a $[Na_2(H_2O)_2]$ unit (Figure 6).

The asymmetric unit of the structure contains just one of these Ru_6 cluster units while the second, symmetry-related unit is generated by the symmetry transformation ($-x + 2$, $-y + 1$, $-z + 1$). The entire unit contains a total of six bridging carbonato ligands that are connected to four Ru atoms each. In all cases two oxygen atoms (O1 and O3) from each of the six carbonate groups coordinate a single Ru atom each, while the third oxygen atom (O2) coordinates two Ru atoms. Carbon−oxygen distances involving oxygen atoms that coordinate just one Ru atom range between 1.265(3) and 1.282(2) Å and are significantly shorter than the ones involving an oxygen atom that coordinates two Ru atoms (1.299(3)−1.304(3) Å). The O−C−O bond angles around C1 of the carbonate group range between 117.9(2)° and 122.1(2)° and deviate only little from the ideal value of 120°.

In the Ru_3 triangle, the bond angles range between 59.380(6)° and 60.442(7)° resulting in an equilateral triangular geometry. In all cases two Ru atoms of the triangle are bridged by one oxygen atom of a carbonato groups. In addition, each of the Ru atoms of the triangle is coordinated by two terminal CO ligands and another Ru atom that is not involved in the Ru_3 triangle.

It should be noted that it was very difficult to properly determine the composition of the cluster by single crystal X-ray diffraction data due to the problem of determining hydrogen positions in the electron density map in the presence of several Ru atoms. The refinement of the structure initially led to a cluster containing six molecules of H_2O and resulted in a composition $[Ru_6(CO_3)_3(CO)_{12}(H_2O)_6][Na_2(H_2O)_2]$. The resulting final electron density map of the Ru cluster showed the presence of residual electron density (1.8 $eÅ^{-3}$) above the triangular Ru_3 faces of the cluster which could be attributed to hydride ligands. However, it was not possible to obtain any evidence for the presence of the face-capping hydride ligand by ^1H NMR spectroscopy. On the other hand, charge-balance considerations for the twelve-membered cluster resulted in a double positive charge for a cluster with the $Ru_{12}C_{30}H_{16}Na_2O_{50}$ that was not being compensated by two negative charges. Close inspection of all hydrogen atoms that were described as water molecules revealed that all would take part in hydrogen bonding. However, it is entirely possible that two of the water molecules are better described as OH groups which might even be disordered in a way that the hydrogen atom of the group is distributed between the two positions, thus simulating the appearance of a water molecule. In order to maintain charge neutrality in the total composition of the compound, we favor the removal of two H^+ from two water molecules that can form Ru−O−Na bridges and the cluster can be described as $[Ru_6(CO_3)_3(CO)_{12}(OH)_2(H_2O)_4][Na_2(H_2O)_2]$. However, more data (neutron diffraction) would be necessary in order to fully determine the nature and composition of this cluster.

Study of the Effect of Surfactants on the Reaction Rate and on the Formation of Ru Species. A series of control experiments were carried out to investigate the effect of surfactants on the reaction rate and the formation of Ru species. Although, the lack of toluene and surfactant did not result in

dx.doi.org/10.1021/cs4007974 | ACS Catal. 2014, 4, 311−320

Table 4. Comparison of Reaction Rates and Selectivity Using Catalyst 1−3

	catalyst[a]	t (°C)	$10^6 \times$ reaction rate ($M \cdot s^{-1}$)	gas composition (%)		
				H_2	CO_2	CO
1	**1**	115	1.210	46.54	50.74	2.72
2	**2**	115	2.060	55.31	42.95	1.74
3	**3**	115	0.703	54.23	37.12	8.66

[a][Catalyst] = 0.424 mM, [FA] = 3.6 M, [HCO_2Na] = 0.4 M, [SDS] = 19.65 mM, 25 mL aqueous solution, 5 mL toluene.

complete inhibition, a significantly lower reaction rate (0.990×10^{-5} $M \cdot s^{-1}$ at 100 °C, Table 3) and selectivity (CO = 0.3%) could be observed. Experiments were also carried out in the absence of surfactant in a water−toluene biphasic system giving a slightly higher reaction rate (1.409×10^{-5} $M \cdot s^{-1}$ at 100 °C) than the one observed in the aqueous phase. The selectivity of the decomposition reaction also increased with only 0.15% CO present in the gaseous phase. Interestingly, in the water−toluene biphasic system, $[Ru_2(HCO_2)_2(CO)_4(PPh_3)_2]$ complex was formed with no traces of any other Ru complexes detected by ^{31}P NMR measurements except for a minor non-characterized species at 13.1 ppm (Supporting Information Figure S7). It also demonstrates the synthetic importance of the method, namely, using FA as both reducing agent and carbonyl source in the preparation of organometallic compounds.

The utilization of an alkylammonium salts such as tetrabutylammonium bromide (TBAB) as a detergent, instead of SDS was also investigated. The reaction rate of the decomposition in the presence TBAB was 2.622×10^{-5} $M \cdot s^{-1}$ (rr = 6.914×10^{-5} $M \cdot s^{-1}$ at 100 °C using SDS). On the basis of the ^{31}P NMR spectrum, $[Ru_2(HCO_2)_2(CO)_4(PPh_3)_2]$ was formed in high yield in addition to some $[Ru(HCO_2)_2(CO)_2(PPh_3)_2]$ and negligible amounts of $[Ru(CO)_3(PPh_3)_2]$ (Supporting Information Figure S8).

Using myristyl trimethylammonium bromide (MiTMAB) resulted in a slightly lower reaction rate (0.958×10^{-5} $M \cdot s^{-1}$ at 100 °C) than the one measured in the absence of surfactant and toluene (0.990×10^{-5} $M \cdot s^{-1}$). Although ^{31}P NMR investigation of the freshly prepared sample revealed the initial presence of $[Ru(CO)_3(PPh_3)_2]$, one day later $[Ru_2(HCO_2)_2(CO)_4(PPh_3)_2]$ was the only Ru-phosphine species present in significant concentration (Supporting Information Figure S9).

It is worth noting that similar to the "ligand free" decomposition of FA in the presence of $RuCl_3$,[18] no decomposition reaction takes place using any of the triphenylphosphine derivatives as ligands under atmospheric pressure regardless of any other reaction parameters, most probably due to low partial pressure of CO that is essential for the formation of the active catalysts.

Comparison of reaction rates and CO contents led us conclude that the addition of surfactants, particularly SDS, significantly increased the activity and the selectivity of the FA decarboxylation and also affected the in situ formation of Ru-carbonyl complexes.

Study of FA Decomposition in the Presence of Complexes 1, 2, and 3. Questions arise whether the isolated Ru complexes **1**−**3** are active catalysts for FA decomposition or the resting states of the active species or simply inactive complexes representing "dead ends" in the catalytic cycle? In order to answer these questions, authentic complexes **1**−**3** were synthesized and used as catalyst for the decarboxylation of FA (Table 4).

Authentic $[Ru(CO)_3(PPh_3)_2]$ (**2**) was synthesized according to a literature method,[36] recrystallized from the mixture of THF and heptanes (1:1) and used as a catalyst for FA decomposition in emulsion (see Experimental Section). Analysis of the product gases (H_2% = 55.31, CO_2% = 42.95, CO% = 1.74) and the observed reaction rate (2.060×10^{-6} M/s at 115 °C) suggested that complex **2** contributes to the catalytic activity to a certain degree but does not give high selectivity. In addition, the ^{31}P NMR study of the crude reaction mixture (Supporting Information Figure S10) revealed the transformation of **2** into $[Ru(HCO_2)_2(CO)_2(PPh_3)_2]$ (**1**) and $[Ru_2(HCO_2)_2(CO)_4(PPh_3)_2]$ (**3**).

$[Ru_2(HCO_2)_2(CO)_4(PPh_3)_2]$ (**3**) was synthesized from $RuCl_3$ in the presence of FA and Na-formate in water/toluene biphasic system in the absence of detergent and the crude material was recrystallized from $CHCl_3$ by hexane diffusion as it was described earlier. It is very unlikely that complex **3** is an active species (or its direct precursor) in the FA decomposition as reflected by the low catalytic activity and poor selectivity (7.027×10^{-7} M/s at 115 °C, H_2%= 54.23, CO_2%= 37.12, CO %= 8.66) which we observed using **3** as a catalyst in emulsion. The low catalytic activity is in accordance with the similar finding of Wills et al.[34] Intact complex **3** could be recovered from the toluene phase after the decomposition reaction, demonstrating the high stability (and most likely low activity) of the complex. Supporting Information Figures S11 and S12 show the comparison of ^{31}P and ^{13}C NMR spectra of **3**, respectively, before and after heating with FA. $[Ru(HCO_2)_2(CO)_2(PPh_3)_2]$ (**1**) was synthesized from $[Ru(CO)_3(PPh_3)_2]$ (**2**) by refluxing in FA following a literature method.[33] Utilization of **1** as a catalyst resulted in moderate activity (1.210×10^{-6} M/s at at 115 °C) and selectivity H_2% = 46.54, CO_2% = 50.74, CO% = 2.72). Supporting Information Figure S13 shows complex **1** was converted to the binuclear $[Ru_2(HCO_2)_2(CO)_4(PPh_3)_2]$ (**3**) upon treating with FA.

One can conclude that isolated and structurally characterized Ru complexes (**1**−**3**) formed in situ from $RuCl_3$ and PPh_3 in the presence of FA do not contribute significantly to the overall catalytic activity. Regardless of their low catalytic activity, the one pot preparation of **1**−**4** from FA without using explosive or toxic gases, such as H_2 and CO, provides a very attractive approach to the synthesis of Ru carbonyls.

Conversion of $[Ru(HCO_2)_2(CO)_2(PPh_3)_2]$ to a Ruthenium Carbonato Complex. Many examples support that a catalyst active for the decomposition of FA may also catalyze the reverse reaction, namely, the formation of FA from CO_2 and H_2 under the reaction conditions.[29,37−39] This could lead to a CO_2 neutral hydrogen storage system.[40] Usually, the addition of bases favors the FA formation (because of the formation of formates) while acidic conditions favor the decomposition. However it must be added here that, from a practical point of view, shifting the unfavorable equilibrium of CO_2 hydrogenation to FA by addition of bases necessitates a further purification step to recover FA from formate salts. On

dx.doi.org/10.1021/cs4007974 | ACS Catal. 2014, 4, 311−320

the other hand, only a few examples for the reduction of CO_2 to FA in the absence of base have been reported.[37] There has also been a very promising progress in isolating FA from amine adducts while minimizing the catalyst loss by using a two phase liquid−liquid system (diol/[$NHex_3$·HCO_2H]−$NHex_3$) as the reaction media.[41] Alternatively, the formate−bicarbonate equilibrium ($HCO_2Na + H_2O \leftrightarrow NaHCO_3 + H_2$) can also be considered to design a carbon-neutral charge−discharge device to store energy.[40,42,43]

We attempted to hydrogenate CO_2 in the presence of $[Ru(HCO_2)_2(CO)_2(PPh_3)_2]$ (**1**) under neutral conditions. The toluene solution of $[Ru(HCO_2)_2(CO)_2(PPh_3)_2]$ was pressurized with the 1:3 mixture of CO_2 and H_2 (460 psi) and the temperature was maintained at 50 °C for 24 h.

Monitoring the pressure of the gas phase showed no consumption of CO_2−H_2 mixture. Furthermore, no FA or any other product of CO_2 reduction could be detected in the reaction mixture. However, the disappearance of the intensive peak at 1611.5 cm^{-1} in the IR spectrum of the crude reaction mixture assigned to monodentate formate ligands in $[Ru(HCO_2)_2(CO)_2(PPh_3)_2]$ and the shift of carbonyl peaks (2053.1 and 1992 cm^{-1}) indicate the formation of a different Ru-carbonyl complex (Scheme 3). Yellow blocks grew from the

Scheme 3. Conversion of $[Ru(HCO_2)_2(CO)_2(PPh_3)_2]$ to $[Ru(CO_3)(CO)_2(PPh_3)_2]$·$H_2O$

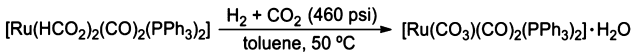

golden yellow solution at room temperature after 3 days. FTIR spectrum of the crystalline material in KBr showed two intensive peaks at 2045.6 and 1982.5 cm^{-1} attributed to carbonyl ligands and three peaks at 1651.3, 1626.7, and 1237.6 cm^{-1} because of bidentate carbonate ligand (Supporting Information Figure S14). High resolution mass spectrometry in a solution of acetonitrile and methanol (1:1) showed a peak at 743.0694 amu which corresponds to MH^+ (where M = $[Ru(CO_3)(CO)_2(PPh_3)_2]$). Single crystals grown from toluene were suitable for X-ray diffraction. The structure of complex $[Ru(CO_3)(CO)_2(PPh_3)_2]$·$H_2O$ is shown in Figure 7.

In accordance with the FTIR spectrum, the X-ray structure determination revealed that the monodentate formate ligand converted to a bidentate carbonate and a water molecule connected to the third oxygen atom of the carbonate ligand by hydrogen bonds. The crystallographic parameters are in good agreement with those available in the literature.[44] It was reported by Calderazzo et al.[44] that $[Ru(CO_3)(CO)_2(PPh_3)_2]$·$H_2O$ can be prepared from a *N,N*-diisopropylcarbamato ruthenium derivative $[Ru(O_2CN^iPr_2)_2(CO)_2(PPh_3)_2]$ by controlled hydrolysis. However, to the best of our knowledge this is the first example of the synthesis of $[Ru(CO_3)(CO)_2(PPh_3)_2]$·$H_2O$ from a ruthenium bisformate.

CONCLUSIONS

Understanding the underlying chemistry of the decomposition of formic acid by identifying the organometallic species formed in situ is essential for the development of robust and recyclable catalysts. We have investigated for the first time the catalytic decomposition of formic acid to hydrogen and carbon dioxide using ruthenium trichloride and triphenylphosphines as catalyst precursors in emulsion and in biphasic (aqueous/organic) systems. It was found that both the activity and the selectivity of

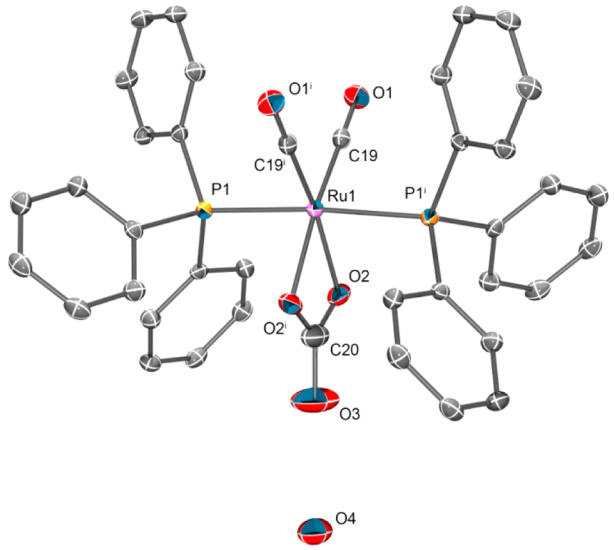

Figure 7. Crystal structure of $[Ru(CO_3)(CO)_2(PPh_3)_2]$·$H_2O$. Hydrogen atoms have been omitted for clarity. Thermal ellipsoids are drawn at the 50% probability level.

the reported catalysts were enhanced by adding surfactants, especially sodium dodecyl sulfate to the toluene/water biphasic system. Ruthenium carbonyls, such as $[Ru(HCO_2)_2(CO)_2(PPh_3)_2]$ (**1**), $[Ru(CO)_3(PPh_3)_2]$ (**2**), and $[Ru_2(HCO_2)_2(CO)_4(PPh_3)_2]$ (**3**), have been isolated from the crude reaction mixtures and structurally characterized. In separate reactions, authentic **1**, **2**, and **3** were synthesized and then used as catalysts for the decarboxylation of formic acid. Based on the presented reaction rates and gas composition data, it can be concluded that these complexes contribute to the overall performance only to a small degree and other substances may account for the observed catalytic activity and selectivity. Despite the low catalytic activity of **1**, **2**, and **3**, the formation of these complexes directly in a reaction between $RuCl_3$ and formic acid in the presence of PPh_3 shows an elegant way for the synthesis of ruthenium formato carbonyls without using explosive and toxic gases such as hydrogen and carbon monoxide. It was also found that the reaction between $RuCl_3$ and O═PPh_3 in the presence of FA and Na-formate resulted in the formation of a novel high nuclearity ruthenium cluster $[Ru_{12}C_{30}H_{14}Na_2O_{50}·6(C_{18}H_{15}OP)·2(C_7H_8)·4(H_2O)]$ (**4**). In the course of the formation of above ruthenium carbonyls FA acted as both reducing and carbonylating agent.

EXPERIMENTAL SECTION

Typical Procedure for the Decomposition of Formic Acid in Emulsion in the Presence of $RuCl_3$ and Triphenylphosphine Catalyst Precursors. Phosphine ligand (0.015 mmol; e.g., 0.0393 g, PPh_3) and 0.590 mmol of emulsifier (e.g., sodium dodecyl sulfate (0.17 g) were mixed in 5.0 mL of toluene and deaerated. In a separate flask nitrogen was bubbled through a mixture of 22.5 mL FA (4.0 M) and 2.5 mL HCO_2Na (4.0 M) for 15 min. Subsequently 0.0156 g (0.073 mmol) $RuCl_3$ was added to the aqueous solution. This mixture was then transferred to the toluene solution under vigorous stirring and the resulting light brown emulsion was sonicated under N_2 for 15 min. The emulsion was then transferred to an autoclave in a glovebox. The autoclave was closed and immersed into a preheated oil bath and heating was continued until the decomposition reached approximately

dx.doi.org/10.1021/cs4007974 | ACS Catal. 2014, 4, 311−320

100% FA conversion. Temperature of the reaction mixture and pressure of the product gases were monitored using Lab View 8.6. The autoclave was allowed to cool down and the gas mixture was vented to a plastic bag from where samples were taken and quantitatively analyzed by gas chromatography and FTIR spectroscopy.

The reaction mixture was separated by centrifugation (4400 rpm, 5 min), extracted with toluene three times and the combined organic layers were dried over anhydrous sodium sulfate. Evaporation of toluene gave a crystalline yellow solid and some yellow oil. ^{13}C and ^{31}P NMR measurements of the crude product were carried out without further purification in $CDCl_3$. Ru-phosphine species identified:

$[Ru(HCO_2)_2(CO)_2(PPh_3)_2]$ (**1**): ^{13}C NMR (100 MHz, $CDCl_3$) (196.7 ppm (t, 11.2 Hz, CO), 167.5 ppm (s, HCO_2^-)); ^{31}P NMR (162 MHz, $CDCl_3$) 31.2 ppm; FTIR (CCl_4, ν_{max}/cm^{-1}) 2052.8, 1991.1, 1957.0 1606.6 and 1300.6. See the FTIR spectrum of $[Ru(HCO_2)_2(CO)_2(PPh_3)_2]$ in Supporting Information Figure S2. $[Ru(CO)_3(PPh_3)_2]$ (**2**): ^{13}C NMR (100 MHz, $CDCl_3$) 208.0 ppm, (t, 16.1 Hz, CO); ^{31}P NMR (162 MHz, $CDCl_3$) 55.6 ppm, FTIR (KBr, ν_{max}/cm^{-1}) 1895. $[Ru_2(HCO_2)_2(CO)_4(PPh_3)_2]$ (**3**): ^{13}C NMR (100 MHz, $CDCl_3$) 204.7 ppm, (t, 4.1 Hz, CO), 176.3 ppm (t, 8.2 Hz, HCO_2^-); ^{31}P NMR (162 MHz, $CDCl_3$) 12.6 ppm.

Crude reaction mixtures were washed with hexane at room temperature three times and the remaining crystalline solid was dissolved in chloroform and hexane was then diffused to the homogeneous solution. The obtained crystals were suitable for X-ray diffraction.

Reaction between $RuCl_3$ and $O{=}PPh_3$ in the Presence of FA and Na−Formate in Aqueous/Toluene. The solution of 0.0885 g (0.318 mmol) of $O{=}PPh_3$ in 5.0 mL of toluene was mixed with the aqueous solution of 0.0330 g (0.154 mmol) of $RuCl_3$ and reacted in a Monel autoclave at 100 °C for 12 h. The reaction mixture was cooled to RT followed by venting of the gaseous mixture of H_2 and CO_2. The yellow-orange toluene phase was separated and the aqueous layer was extracted with toluene three times. Orange-red crystals formed from the aqueous phase by next day which were suitable for X-ray structural determination.

$[Ru_{12}C_{30}H_{14}Na_2O_{50}{\cdot}6(C_{18}H_{15}OP){\cdot}2(C_7H_8){\cdot}4(H_2O)]$ (**4**): ^{13}C NMR (100 MHz, CD_3OD) 162.3 ppm (CO_3), 181.4 ppm (CO); ^{31}P NMR (162 MHz, CD_3OD) 28.8 ppm; FTIR (KBr, cm^{-1}) 2050.7, 2022.5, 1987.5, 1956.0, 1922.4, 1540.4.

Conversion of $[Ru(HCO_2)_2(CO)_2(PPh_3)_2]$ to $[Ru(CO_3)(CO)_2(PPh_3)_2]{\cdot}H_2O$. Nitrogen was bubbled through a mixture of 22.5 mL of FA (4.0 M) and 2.5 mL of HCO_2Na (4.0 M) for 15 min and then 0.0468 g (0.219 mmol) of $RuCl_3$ was added. PPh_3 (0.118 g, 0.45 mmol) and 0.51 g (1.770 mmol) of SDS was dissolved in 5 mL of toluene. The toluene solution was deaerated and the aqueous solution was added under vigorous stirring and sonicated under N_2 for 15 min. The emulsion was transferred to an autoclave and pressurized with CO (30 psi). The reaction mixture was kept at 90 °C for 17 h and then the organic layer was dried under reduced pressure. (Note: Since the FTIR analysis of the crude product confirmed the formation of complex **1**, it was used for the next step without further purification.)

The yellow solid was transferred to an autoclave and dissolved in 15 mL of toluene and a 1:3 mixture of CO_2 and H_2 (460 psi) was added. The temperature was maintained at 50 °C for 24 h. Small brown particles were removed with a syringe filter and the obtained golden yellow solution was kept in a vial for 3 days. The yellow cubes were filtered from the brown mother liquor and washed with a few drops of toluene and then with hexane at 0 °C. Yield: 0.086 g (50.3%). $[Ru(CO_3)(CO)_2(PPh_3)_2]{\cdot}H_2O$: FTIR (KBr, ν_{max}/cm^{-1}) 2045.6, 1982.5, 1651.3, 1626.7, and 1237.6 cm^{-1}; HRMS in acetonitrile-methanol (1:1) 743.0694 MH^+ (where M = $[Ru(CO_3)(CO)_2(PPh_3)_2]$).

■ ASSOCIATED CONTENT

Ⓢ Supporting Information

Details for crystal structure determination, crystallographic parameters, a typical gas chromatogram, FTIR spectra, ^1H, ^{13}C, and ^{31}P NMR spectra are given. This material is available free of charge via the Internet at http://pubs.acs.org.

■ AUTHOR INFORMATION

Corresponding Authors

*Fax: (+)1 213 740 5087. E-mail: czaun@usc.edu.
*Fax: (+)1 213 740 5087. E-mail: gprakash@usc.edu.
*Fax: (+)1 213 740 5087. E-mail: olah@usc.edu.

Notes

The authors declare no competing financial interest.

■ ACKNOWLEDGMENTS

Support of our work by the Loker Hydrocarbon Research Institute and the U.S. Department of Energy is gratefully acknowledged. We also acknowledge NSF CRIF grant 1048807 for the purchase of a X-ray diffractometer.

■ REFERENCES

(1) Harvey, F. *The Guardian* **2011**, May 29.
(2) Olah, G. A.; Goeppert, A.; Prakash, G. K. S. *J. Org. Chem.* **2009**, *74*, 487.
(3) Olah, G. A.; Prakash, G. K. S.; Goeppert, A. *J. Am. Chem. Soc.* **2011**, *133*, 12881.
(4) Olah, G. A.; Goeppert, A.; Czaun, M.; Prakash, G. K. S. *J. Am. Chem. Soc.* **2012**, *135*, 648.
(5) Olah, G. A.; Prakash, G. K. S.; Goeppert, A.; Czaun, M.; Mathew, T. *J. Am. Chem. Soc.* **2013**, *135*, 10030.
(6) Olah, G. A.; Goeppert, A.; Prakash, G. K. S. *Beyond Oil and Gas: The Methanol Economy*, 2nd ed.; Wiley VCH: Weinheim, Germany, 2009.
(7) Conley, B. L.; Guess, D.; Williams, T. J. *J. Am. Chem. Soc.* **2011**, *133*, 14212.
(8) Jiang, H. L.; Singh, S. K.; Yan, J. M.; Zhang, X. B.; Xu, Q. *ChemSusChem* **2010**, *3*, 541.
(9) Tanaka, N. *Potential for Biomass and Carbon Dioxide Capture and Storage*; International Energy Agency Environmental Projects Ltd.: London, 2011.
(10) Aresta, M. *Carbon Dioxide as Chemical Feedstock*; Wiley-VCH: Weinheim, Germany, 2010.
(11) Federsel, C.; Jackstell, R.; Beller, M. *Angew. Chem., Int. Ed.* **2010**, *49*, 6254.
(12) Federsel, C.; Jackstell, R.; Boddien, A.; Laurenczy, G.; Beller, M. *ChemSusChem* **2010**, *3*, 1048.
(13) Agarwal, A. S.; Zhai, Y.; Hill, D.; Sridhar, N. *ChemSusChem* **2011**, *4*, 1301.
(14) Prakash, G. K. S.; Viva, F. A.; Olah, G. A. *J. Power Sources* **2013**, *223*, 68.
(15) Keene, F. R. *Electrochemical and Electrocatalytic Reactions of Carbon Dioxide*; Elsevier: Amsterdam, 1993.
(16) Boddien, A.; Loges, B.; Junge, H.; Beller, M. *ChemSusChem* **2008**, *1*, 751.
(17) Joo, F. *ChemSusChem* **2008**, *1*, 805.

(18) Czaun, M.; Goeppert, A.; May, R.; Haiges, R.; Prakash, G. K. S.; Olah, G. A. *ChemSusChem* **2011**, *4*, 1241.
(19) Loges, B.; Boddien, A.; Gartner, F.; Junge, H.; Beller, M. *Top. Catal.* **2010**, *53*, 902.
(20) Fellay, C.; Dyson, P. J.; Laurenczy, G. *Angew. Chem., Int. Ed.* **2008**, *47*, 3966.
(21) Boddien, A.; Mellmann, D.; Gaertner, F.; Jackstell, R.; Junge, H.; Dyson, P. J.; Laurenczy, G.; Ludwig, R.; Beller, M. *Science* **2011**, *333*, 1733.
(22) Grasemann, M.; Laurenczy, G. *Energy Environ. Sci.* **2012**, *5*, 8171.
(23) Hull, J. F.; Himeda, Y.; Wang, W. H.; Hashiguchi, B.; Periana, R.; Szalda, D. J.; Muckerman, J. T.; Fujita, E. *Nat. Chem.* **2012**, *4*, 383.
(24) Czaun, M.; Goeppert, A.; May, R. B.; Peltier, D.; Zhang, H.; Prakash, G. K. S.; Olah, G. A. *J. CO_2 Util.* **2013**, *1*, 1.
(25) Goeppert, A.; Meth, S.; Prakash, G. K. S.; Olah, G. A. *Energy Environ. Sci.* **2010**, *3*, 1949.
(26) Meth, S.; Goeppert, A.; Prakash, G. K. S.; Olah, G. A. *Energy Fuels* **2012**, *26*, 3082.
(27) Goeppert, A.; Czaun, M.; May, R. B.; Prakash, G. K. S.; Olah, G. A.; Narayanan, S. R. *J. Am. Chem. Soc.* **2011**, *133*, 20164.
(28) Goeppert, A.; Czaun, M.; Surya Prakash, G. K.; Olah, G. A. *Energy Environ. Sci.* **2012**, *5*, 7833.
(29) Loges, B.; Boddien, A.; Junge, H.; Beller, M. *Angew. Chem., Int. Ed.* **2008**, *47*, 3962.
(30) Shin, J. H.; Yoon, J. H.; Lee, S. H.; Park, T. H. *Bioresour. Technol.* **2010**, *101*, S53.
(31) Sponholz, P.; Mellmann, D.; Junge, H.; Beller, M. *ChemSusChem* **2013**, *6*, 1172.
(32) Laurenczy, G.; Fellay, C.; Yan, N.; Dyson, P. J. *Chem.—Eur. J.* **2009**, *15*, 3752.
(33) Johnson, B. F. G.; Johnston, R. D.; Lewis, J.; Williams, I. G. *J. Chem. Soc. A* **1971**, 689.
(34) Morris, D. J.; Clarkson, G. J.; Wills, M. *Organometallics* **2009**, *28*, 4133.
(35) Collman, J. P.; Roper, W. R. *J. Am. Chem. Soc.* **1965**, *87*, 4008.
(36) Ahmad, N.; Levison, J. J.; Robinson, S. D.; Uttlky, M. F.; Wonchoba, E. R.; Parshall, G. W. In *Inorganic Syntheses*; John Wiley & Sons, Inc.: Hoboken, NJ, 2007; Vol. *15*, p 45.
(37) Hayashi, H.; Ogo, S.; Fukuzumi, S. *Chem. Commun.* **2004**, 2714.
(38) Himeda, Y. *Green Chem.* **2009**, *11*, 2018.
(39) Gao, Y.; Kuncheria, J. K.; Jenkins, H. A.; Puddephatt, R. J.; Yap, G. P. A. *J. Chem. Soc., Dalton Trans.* **2000**, 4703.
(40) Boddien, A.; Gaertner, F.; Federsel, C.; Sponholz, P.; Mellmann, D.; Jackstell, R.; Junge, H.; Beller, M. *Angew. Chem., Int. Ed.* **2011**, *50*, 6411.
(41) Schaub, T.; Paciello, R. A. *Angew. Chem., Int. Ed.* **2011**, *50*, 7278.
(42) Zaidman, B.; Wiener, H.; Sasson, Y. *Int. J. Hydrogen Energy* **1986**, *11*, 341.
(43) Papp, G.; Csorba, J.; Laurenczy, G.; Joo, F. *Angew. Chem., Int. Ed.* **2011**, *50*, 10433.
(44) Dell'Amico, D. B.; Calderazzo, F.; Labella, L.; Marchetti, F. *J. Organomet. Chem.* **2000**, *596*, 144.